NETWORKED MODEL PREDICTIVE CONTROL FOR SATELLITE FORMATION FLYING

Damiana Catanoso[*], Florian Kempf[†], Klaus Schilling[‡] and Simone D'Amico[§]

A novel continuous low-thrust fuel-efficient model predictive control strategy for N-satellite formations flying in low earth orbit is presented. State prediction relies on a full nonlinear relative motion model, based on quasi-nonsingular relative orbital elements, admitting reference orbits of arbitrary eccentricity, including earth oblateness effects and, through state augmentation, differential drag. The optimal control problem is specifically designed to incorporate latest theoretical results concerning maneuver optimality in the state-space, yielding to a sensible total ΔV reduction, while assuring feasibility and stability though imposition of a Lyapunov constraint. The controller is particularly suitable for networked architectures since it exploits the predictive strategy and the dynamics knowledge to provide robustness against feedback data losses and delays. A Lagrangian augmented gradient-based algorithm provides iterative solution to the optimal control problem. Controller validation has been conducted using the high fidelity orbit propagator developed by the Space Rendezvous Laboratory.

INTRODUCTION

Distributed Space Systems (DSS) rely on the use of multi-agents formations or swarms to replace large space-borne architectures, improving achievable mission outcomes while lowering costs. Demonstration missions, such as TanDEM-X and PRISMA,[1] successfully validated autonomous relative navigation and control technology, encouraging an increase in complexity and technological evolution. Zentrum fuer Telematik recently took up the miniaturization challenge with the NetSat mission, mounting electric actuators on a 1U CubeSat for low earth orbit (LEO) control.[2] The Telematik earth Observation Mission (TOM) will fly three 3U CubeSats in a triple pendulum configuration to provide 3D images of volcanic ash clouds.[3] The Space Rendezvous Laboratory (SLAB) is looking at the use of DSS for observation of the universe and exploration of the solar system through the two-spacecraft occulter/telescope mDOT, which will detect zodiacal dust orbiting around nearby stars,[4] and the Autonomous Nanosatellite Swarming (ANS) mission aimed at characterizing asteroids.[5]

Satellite modular architectures currently have wired communication among subsystems and will possibly evolve into fractionated architectures, where modules communicate wirelessly, in a net-

[*]Research Scholar, Stanford University, Dept. of Aeronautics and Astronautics, Space Rendezvous Laboratory, Durand Building, 496 Lomita Mall, Stanford, CA 94305-4035. Email: damianac@stanford.edu

[†]Doctoral Candidate, University of Wuerzburg, Dept. of Computer Sciences, Am Hubland, 97074 Wuerzburg, Germany. Email: kempf@informatik.uni-wuerzburg.de

[‡]Professor, University of Wuerzburg, Dept. of Computer Sciences, Am Hubland, 97074 Wuerzburg, Germany. Email: schi@informatik.uni-wuerzburg.de

[§]Assistant Professor, Stanford University, Dept. of Aeronautics and Astronautics, Space Rendezvous Laboratory, Durand Building, 496 Lomita Mall, Stanford, CA 94305-4035. Email: damicos@stanford.edu

worked fashion. A clear advantage of such architecture for satellite formation flying is the possibility for a neighboring satellite to take over control authority of one satellite's sensors and actuators in the event of faults in the control unit. Satellite swarms relying on intensive sensors and actuators data flow represent networked architectures as well. Being networked structures based on long-distance wireless data exchange and disturbed short-distance communication, they should be able to maintain acceptable closed-loop performance in the presence of data losses and delays while guaranteeing minimum fuel expenditure, which is of paramount importance in the space domain. Control requirements imposed by design of a networked control strategy appear to be fully met by model predictive control (MPC). With its intrinsic knowledge of the system dynamics and the iterative computation of a fuel optimal control sequence for the entire length of the prediction horizon,[6,7] MPC is able to control the system in an open-loop fashion in case of losses in the feedforward direction. Extended faults or delays in the feedback direction can be compensated replacing missing measurements with state estimates obtained through propagation. Additionally, MPC allows for easy incorporation of state and control constraints, as well as minimum ΔV requirements, representing a suitable candidate for the proposed solution.[8]

Several studies appearing in literature employ MPC to solve the satellites' relative motion control problem. Most of them utilize the Hill-Clohessy-Wiltshire (HCW) model, which uses relative position and velocity as state vector.[9–13] The HCW dynamic model, which is not accurate for large separations, assumes a circular reference orbit and neglects orbital perturbations. Larsson et. al. incorporate the Yamanaka-Ankersen (YA) State Transition Matrix (STM) in the dynamics to account for eccentric reference orbits.[14] Hartley et. al. designed a three-stages MPC for docking maneuvers. For small separations, they adopt the YA model, while for long distances a nonsingular relative orbital elements (ROE)-based representation, derived from the linearized Gauss Variational Equations (GVEs), is used.[15] Nonlinear dynamics reduction to a linear model and constraints linearization appearing in literature are motivated by the desire of reducing the optimal control problem (OCP) to a linear quadratic regulator (LQR),[10] quadratic programming (QP) problem,[9] or a linear programming problem (LP),[14] which, under certain circumstances, can be solved explicitly.[10,12,13] When reducing the problem to an LQR or LP, traditional stability arguments, based on terminal set constraints and terminal cost, can be employed to prove convergence and stability.

Based on a predictive control strategy, this work proposes a novel ROE-based continuous low-thrust fuel-optimal control approach for a N-satellite formation flying in LEO orbits of arbitrary eccentricity, which is also robust against feedback delays/losses. The first contribution to the state of the art involves introduction of a non-linearized relative motion model in the MPC formulation, in order to guarantee high accuracy for arbitrary separations and reference orbit type. This leads however to a nonconvex optimization problem, which in general only provides a sub-optimal solution. To improve efficiency of the solution, a second innovation is presented in this work: the d-term. The d-term allows exploitation of the latest theoretical results in terms of the properties of a fuel-optimal trajectory in ROE-space. The novel term is included in the cost function and drives the MPC solution to resemble the optimal closed-form solution behavior. Compared to impulsive closed-form solutions, which require a given amount of orbits to execute any maneuver, the continuous MPC solution is more versatile and suitable for time-constrained applications. For the optimal control problem solution, a warm start strategy is adopted to avoid incursion in local minima which are excessively far from the global optimum. The initial solution guess consists of the convex OCP solution, obtained by replacing the nonlinear model with the linearized one. The OCP solution is then calculated using a gradient based augmented Lagrangian approach with customiz-

able number of maximum iterations, which allows to control the execution time.[16] Relative orbital elements, instead of relative position and velocity, as state representation allows the use of a larger integration time interval, relieving the algorithm from excessive computational intensity. Given the difficulties of employing traditional stability arguments for a nonlinear time-varying model affected by uncertainties, feasibility and stability are achieved through imposition of a Lyapunov inequality constraint.[17] The optimal control trajectory, which provides optimal input for the entire prediction horizon length, is used to keep implementing a control action in the event of absence of new state information. If no new measurements are detected for more than one prediction window, a state estimate is used to calculate a new optimal solution.

Following this introduction, the ROE-based nonlinear dynamics derivation is presented. Next, the controller architecture including the delays/losses compensation structure and the optimal control problem formulation is explained. The last section presents results of a set of simulation scenarios aimed at validating the controller through high fidelity orbital propagation.

NONLINEAR DYNAMICS

The relative motion of a deputy satellite with respect to the chief is described in the Local-Vertical Local-Horizontal (**RTN**) rotating frame, centered on the chief satellite or a virtual reference point. The **R** axis is pointing along the chief orbital radius, the **N** axis is pointing along its angular momentum vector and **T** is obtained performing the cross product $\mathbf{T} = \mathbf{N} \times \mathbf{R}$. The quasi-nonsingular relative orbital elements define the relative state as

$$\delta\boldsymbol{\alpha} = \begin{pmatrix} \delta a \\ \delta\lambda \\ \delta e_x \\ \delta e_y \\ \delta i_x \\ \delta i_y \end{pmatrix} = \begin{pmatrix} \delta a \\ \delta\lambda \\ \delta e\, cos\, \sigma \\ \delta e\, sin\, \sigma \\ \delta i\, cos\, \theta \\ \delta i\, sin\, \theta \end{pmatrix} = \begin{pmatrix} (a - a_c)/a_c \\ \varphi - \varphi_c + (\Omega - \Omega_c)\, cos\, i_c \\ e\, cos\, \omega - e_c\, cos\, \omega_c \\ e\, sin\, \omega - e_c\, sin\, \omega_c \\ i - i_c \\ (\Omega - \Omega_c)\, sin\, i_c \end{pmatrix}. \tag{1}$$

They are a nonlinear combination of the deputy's and chief's absolute orbital elements. In Equation 1, variables relative to the chief spacecraft are labeled with the subscript c, while the absence of a subscript refers to the deputy. M is the mean anomaly and $\varphi = \omega + M$ defines the mean argument of latitude. Compared to the relative position and velocity representation, the relative orbital elements allow easy incorporation of the J2 and differential drag perturbations, as well as passive collision avoidance through the eccentricity/inclination vector separation.[18] They also provide a more intuitive perception of the geometric features of the formation.[19] Furthermore, the quasi-nonsingular ROE, which are not uniquely defined for equatorial reference orbits, coincide with the integration constants of the HCW equations for near-circular orbit and the Tschauner−Hempel equations for eccentric orbits.[20] Inaccuracies in the atmospheric density characterization using available models motivate the choice of state augmentation for differential drag inclusion. The augmented state vector

$$\delta\bar{\boldsymbol{\alpha}} = \begin{bmatrix} \delta\boldsymbol{\alpha} \\ \delta\dot{a}_d \\ \delta\dot{e}_{xd} \\ \delta\dot{e}_{yd} \end{bmatrix} \tag{2}$$

contains three additional terms representing the rates of change due to differential drag of the elements affected by the orbit perturbation: $\delta\dot{a}_d$, $\delta\dot{e}_{xd}$, $\delta\dot{e}_{yd}$. It is worth mentioning that $\delta\dot{a}_d$ has

generally a greater order of magnitude than $\delta\dot{\boldsymbol{e}}_d$, whose accurate on-board estimation is achievable only in LEO. Hence, at higher altitudes, it is convenient to augment the state only with $\delta\dot{a}_d$ and express $\delta\dot{\boldsymbol{e}}_d$ as a function of $\delta\dot{a}_d$.

Model Derivation

The absolute motion of a spacecraft subject to control accelerations and secular J2 drifts is given by

$$\dot{\text{oe}} = \dot{\text{oe}}_K + \dot{\text{oe}}_u + \dot{\text{oe}}_{J2}, \tag{3}$$

where oe represents the absolute orbital elements vector and the subscripts K, u and $J2$ refer to the motion components respectively due to: Keplerian dynamics

$$\dot{\text{oe}}_K = \frac{d}{dt}\begin{pmatrix} a \\ e \\ i \\ \Omega \\ \omega \\ M \end{pmatrix}_K = \begin{pmatrix} 0 \\ 0 \\ 0 \\ 0 \\ 0 \\ n \end{pmatrix}, \tag{4}$$

control input vector

$$\dot{\text{oe}}_u = \frac{d}{dt}\begin{pmatrix} a \\ e \\ i \\ \Omega \\ \omega \\ M \end{pmatrix}_u = \begin{pmatrix} \frac{2a^2 e\sin f}{h} & \frac{2a^2 p}{rh} & 0 \\ \frac{p\sin f}{h} & \frac{(p+r)\cos f + re}{h} & 0 \\ 0 & 0 & \frac{r\cos\theta}{h} \\ 0 & 0 & \frac{r\sin\theta}{h\sin i} \\ -\frac{pcosf}{he} & \frac{(p+r)sinf}{he} & -\frac{r\sin\theta\cos i}{h\sin i} \\ \frac{b(p\cos f - 2re)}{ahe} & -\frac{b(p+r)\sin f}{ahe} & 0 \end{pmatrix} \begin{pmatrix} u_r \\ u_t \\ u_n \end{pmatrix}, \tag{5}$$

and secular J2 effect[21]

$$\dot{\text{oe}}_{J2} = \frac{d}{dt}\begin{pmatrix} a \\ e \\ i \\ \Omega \\ \omega \\ M \end{pmatrix}_{J2} = \frac{3}{4}\frac{J_2 R_E^2\sqrt{\mu}}{a^{7/2}\eta^4}\begin{pmatrix} 0 \\ 0 \\ 0 \\ -2\cos(i) \\ 5\cos^2(i) - 1 \\ \eta(3\cos^2(i) - 1) \end{pmatrix} \tag{6}$$

The sum of Equations 4 and 5 are the well known Gauss Variational Equations for a satellite subject to the sole control acceleration vector $\boldsymbol{u}$.[22] In order to derive the model, it is here assumed that only the deputy is subject to control accelerations. The chief spacecraft motion is obtained neglecting the $\dot{\text{oe}}_u$ contribution in Equation 3. Differentiating Equation 1 with respect to time yields to the expression of the desired relative dynamic model as a function of oe_c, oe_d, $\dot{\text{oe}}_c$ and $\dot{\text{oe}}_d$. The rate of change of the chief and deputy orbital elements are replaced with the respective GVEs expression.

$\mathbf{oe}_d$ is written as a function of $\mathbf{oe}_c$ and ROE, according to

$$\mathbf{oe}_d = \begin{pmatrix} a_d \\ e_d \\ i_d \\ \Omega_d \\ \omega_d \\ M_d \end{pmatrix} = \begin{pmatrix} a_c \delta a + a_c \\ \Omega_c + \frac{\delta i_y}{\sin i_c} \\ \sqrt{(e_c \cos\omega_c + \delta e_x)^2 + (e_c \sin\omega_c + \delta e_y)^2} \\ i_c + \delta i_x \\ tan^{-1}(\frac{e_c \sin\omega_c + \delta e_y}{e_c \cos\omega_c + \delta e_x}) \\ M_c + \delta\lambda - (\omega_d - \omega_c) - (\Omega_d - \Omega_c)\cos i_c \end{pmatrix}. \tag{7}$$

The first order system of differential equations, governing the J2-perturbed evolution of the relative orbital elements is obtained. The last step of including differential drag is performed replacing the state vector $\delta\boldsymbol{\alpha}$ with the augmented $\delta\bar{\boldsymbol{\alpha}}$ and adding differential drag contributions $\delta\dot{a}_d$, $\delta\dot{e}_{xd}$ and $\delta\dot{e}_{yd}$ to the right-hand side of the system of equations. The resulting full dynamics is compactly expressed as

$$\delta\dot{\bar{\boldsymbol{\alpha}}} \;=\; \boldsymbol{F}(\mathbf{oe}_c, \delta\bar{\boldsymbol{\alpha}}, \boldsymbol{u}) \;=\; \begin{bmatrix} \boldsymbol{f}(\mathbf{oe}_c, \delta\bar{\boldsymbol{\alpha}}) + \boldsymbol{B}(\mathbf{oe}_c, \delta\boldsymbol{\alpha})\,\boldsymbol{u} \\ \mathbf{0}^{3x1} \end{bmatrix}. \tag{8}$$

CONTROLLER STRUCTURE

Characterization of an optimal control problem starts with defining the controlled system dynamics, a proper objective function, as well as state and control constraints. Once the OCP is defined, model predictive control provides solution to the finite horizon control problem, which represents a sub-optimal solution to the infinite time optimal control problem, obtained theoretically extending the prediction horizon length to infinity.[23] Before selecting a proper solution technique, it is good practice to study the OCP convexity properties, in order to establish and prove criteria for MPC stability and OCP feasibility, a priori. In general, a convex optimal control problem is characterized by a convex cost function defined over state and control convex sets.[24] The model is a constraint, convex if linear. In presence of particularly simplified convex problems, such as Linear Regulators and Linear Quadratic Regulators, introduction of a terminal set constraint and a terminal cost are typical ways of proving MPC feasibility and stability.[7] When the system is characterized by uncertainties, such properties can be guaranteed through adoption of robust control invariant sets theory.[23] In this paper, adoption of uncertain, nonlinear and time-variant dynamics yields to difficulties in using the previously mentioned criteria for stability proof. Hence, stability and feasibility are here achieved through addition of a further inequality constraint, formulated by means of Lyapunov theory.

Optimal Control Problem

The optimal control problem, defined as

$$\min_{\boldsymbol{u}\in[\boldsymbol{u}_{min},\boldsymbol{u}_{max}]} \quad \int_{t_k}^{t_k+N\Delta t} [\,\|\Delta\delta\boldsymbol{\alpha}(\tau)\|_Q + \|\boldsymbol{u}(\tau)\|_R + \|\boldsymbol{d}(\tau)\|_S\,]\,d\tau \tag{9a}$$

$$\text{s.t.} \quad \delta\bar{\boldsymbol{\alpha}}(t_k) = \delta\bar{\boldsymbol{\alpha}}_k \tag{9b}$$

$$\delta\dot{\bar{\boldsymbol{\alpha}}}(t) \;=\; \boldsymbol{F}(\mathbf{oe}_c(t), \delta\bar{\boldsymbol{\alpha}}(t), \boldsymbol{u}(t)) \tag{9c}$$

$$h(\delta\boldsymbol{\alpha}, t) \leq 0 \qquad \forall t \in [t_k, t_k + N\Delta t], \tag{9d}$$

is solved at each time step t_k using the measured state $\delta\bar{\boldsymbol{\alpha}}_k$ as initial condition (Equation 9b). Equation 9c represents the nonlinear dynamics, derived in the previous section, and Equation 9d the Lyapunov constraint. A box constraint forces the control input to belong to the given interval

$[\boldsymbol{u}_{min}, \boldsymbol{u}_{max}]$, as shown in Equation 9a. The tracking error term $\Delta\delta\boldsymbol{\alpha}$ is included in the cost function to achieve convergence to the target state. The two further terms appearing in the cost aim at achieving maneuver efficiency respectively through penalization of the control input effort and exploitation of optimality features of the state trajectory in ROE space. In particular, the vector indicated with $\boldsymbol{d}$ in Equation 9a, defined as

$$\boldsymbol{d} = [d_{\delta \boldsymbol{e}},\ d_{\delta \boldsymbol{i}}]^\top, \tag{10}$$

represents the distance between the current state, respectively in $\delta\boldsymbol{e}$ and $\delta\boldsymbol{i}$ space, and the straight line connecting initial and target states, as illustrated in Figure 1. In Reference 25, Chernick et.

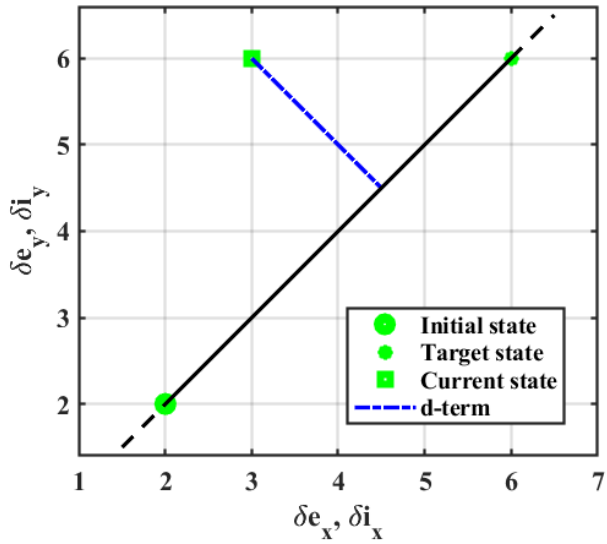

Figure 1. ROE-space geometric representation of the d-term as the distance between the state and the line connecting initial and target state, representing the fuel-optimal trajectory.

al. show that, for a cross-track maneuver, optimality in relative inclination space corresponds to the minimum path trajectory from the initial $\delta\boldsymbol{i}_0$ to the target $\delta\boldsymbol{i}_t$ state. Same behavior is observed for a fuel-optimal in-plane maneuver in relative eccentricity space where the tracking error in $\delta\boldsymbol{e}$ dominates over the error in δa, i. e. $||\Delta\delta\boldsymbol{e}|| > |\Delta\delta a|$. Equation 10 is referred as "d-term".

The Lyapunov constraint is introduced to provide a sufficient condition for feasibility and stability. Supposing a stabilizing Lyapunov control law $\tilde{\boldsymbol{u}}$, whose values range within the given box constraint boundaries, exists for the system, it follows that it represents a feasible solution. Being $\delta\tilde{\boldsymbol{\alpha}}$ the state resulting when $\tilde{\boldsymbol{u}}$ is applied, and being V the Lyapunov function used to derive $\tilde{\boldsymbol{u}}$, it follows that $V(\delta\tilde{\boldsymbol{\alpha}})$ decreases with time. Constraining the Lyapunov function $V(\delta\boldsymbol{\alpha})$, where $\delta\boldsymbol{\alpha}$ is the MPC-controlled system state, to decrease at the same rate of $V(\delta\tilde{\boldsymbol{\alpha}})$ or faster, the MPC-controlled system inherits stability properties from the stabilizing control law $\tilde{\boldsymbol{u}}$.[17] Given the Lyapunov function candidate for the system of Equation 9c

$$V = \frac{1}{2}\Delta\delta\boldsymbol{\alpha}^\top\Delta\delta\boldsymbol{\alpha}, \tag{11}$$

imposing its derivative to be negative

$$\dot{V} = -\Delta\delta\boldsymbol{\alpha}^\top\boldsymbol{P}\Delta\delta\boldsymbol{\alpha}, \tag{12}$$

it results

$$\dot{V} = \Delta\delta\boldsymbol{\alpha}^\top \Delta\delta\dot{\boldsymbol{\alpha}} = \Delta\delta\boldsymbol{\alpha}^\top \delta\dot{\boldsymbol{\alpha}} = \Delta\delta\boldsymbol{\alpha}^\top [\, \boldsymbol{f} + \boldsymbol{B}\, \boldsymbol{u}\,] = -\Delta\delta\boldsymbol{\alpha}^\top \boldsymbol{P} \Delta\delta\boldsymbol{\alpha}\ . \tag{13}$$

The control law $\tilde{\boldsymbol{u}}$ is obtained and given by

$$\tilde{\boldsymbol{u}} = -\boldsymbol{B}^* \left[\boldsymbol{P}\Delta\delta\boldsymbol{\alpha} + \boldsymbol{f}\right] , \tag{14}$$

where $\boldsymbol{B}^*$ represents the pseudo-inverse of the control input matrix. When $\tilde{\boldsymbol{u}}$ is applied to the system of Equation 8, the resulting dynamics becomes:

$$\delta\dot{\tilde{\boldsymbol{\alpha}}} = -\boldsymbol{P}\, \Delta\delta\boldsymbol{\alpha}\ . \tag{15}$$

The feedback gain matrix $\boldsymbol{P}$ is designed to intensify the thrust effort in proximity of the most fuel-efficient locations along the reference orbit. $\boldsymbol{P}$ is given by[26]

$$\boldsymbol{P} = \frac{1}{k} \begin{pmatrix} cos(J)^N & 0 & 0 & 0 & 0 & 0 \\ 0 & cos(J)^N & 0 & 0 & 0 & 0 \\ 0 & 0 & cos(J)^N & 0 & 0 & 0 \\ 0 & 0 & 0 & cos(J)^N & 0 & 0 \\ 0 & 0 & 0 & 0 & cos(H)^N & 0 \\ 0 & 0 & 0 & 0 & 0 & cos(H)^N \end{pmatrix} , \tag{16}$$

where the cosine's arguments are $J = \varphi - \bar{\varphi}_{ip}$, for the in-plane case, and $H = \varphi - \bar{\varphi}_{oop}$, for the out-of-plane.[26] The optimal locations $\bar{\varphi}_{ip}$ and $\bar{\varphi}_{oop}$ for perturbed near-circular orbits and unperturbed eccentric orbits can be calculated according to the results presented in Reference 25. Computation of the in-plane optimal location in the eccentric orbit case involves the use of an iterative numerical method, which is not desirable when the calculation has to be performed at each time-step. Hence, for the sake of computational efficiency, it is here chosen to include the simplified expression of $\bar{\varphi}_{ip}$ and $\bar{\varphi}_{oop}$ for unperturbed near-circular orbits, given by:[26]

$$\bar{\varphi}_{ip} = atan2\left(\frac{\Delta\delta e_y}{\Delta\delta e_x}\right) , \tag{17}$$

$$\bar{\varphi}_{oop} = atan2\left(\frac{\Delta\delta i_y}{\Delta\delta i_x}\right) . \tag{18}$$

In the feedback gain matrix, the value of the tuning variable k is chosen to prevent $\tilde{\boldsymbol{u}}$ from exceeding the limits imposed by the box constraint. N is a positive even number that regulates the width of the cosine-shaped impulse. Recalling that $\delta\tilde{\boldsymbol{\alpha}}$ represents the system state controlled by the Lyapunov law $\tilde{\boldsymbol{u}}$ of Equation 15, the Lyapunov constraint is given by

$$h = V(\delta\boldsymbol{\alpha}) - V(\delta\tilde{\boldsymbol{\alpha}}) \leq 0 \qquad t \in [t_k,\ t_k + N\Delta t]. \tag{19}$$

It is worth noting that the Lyapunov constraint is a quadratic and convex function of the state, where control variables do not appear. The control input vector is exclusively subject to the convex box constraint. However due to the nonlinear model, the OCP defined in Equations 9a-9d is a nonconvex problem.

Data Delays/Losses Compensation Structure

According to the receding horizon strategy, at each time step, the finite horizon optimal control problem is repetitively solved, the first solution set is applied to the system and the rest discarded. In the event of feedback deficiencies, delays and losses in the acquisition of feedback data yield to absence of the OCP initial condition, which cannot be solved at the desired synchronous pace. To prevent the spacecraft from drifting uncontrolled, the conventional MPC algorithm is here augmented with a delays/losses compensation structure, whose block diagram is presented in Figure 2. It is assumed that a feedback data package received at time t_k contains state information $\delta\boldsymbol{\alpha}_{FB}$ relative to a known time t_{FB}. At time t_k the algorithm reads the values of $\delta\boldsymbol{\alpha}_{FB}$ and t_{FB} variables and compares them with the last received measurement $\delta\boldsymbol{\alpha}_x$, relative to t_x: if new values are detected, new data has arrived. If the new measurement refers to a time prior to the last received measurement, the data is discarded. If the measurement refers to a past state and brings new information, estimation of the current state $\delta\boldsymbol{\alpha}_k$ is obtained integrating the model from the last valid measured state until time t_k. The measured or estimated current state is fed as initial condition into the OCP block, which provides a sequence of optimal control inputs $\boldsymbol{u}^*$ for the entire length of the prediction horizon T. Suppose at the next time-step no new measurements are detected, i. e. it is not possible to execute the OCP block, the controller implements the next available optimal $\boldsymbol{u}$ from the previously calculated optimal control sequence $\boldsymbol{u}^*$. If the absence of feedback persists, subsequent elements of $\boldsymbol{u}^*$ are extracted. When all $\boldsymbol{u}^*$ elements have been implemented, a new state estimate is calculated using the dynamics and the applied control history. This is then used as initial condition to provide a new OCP solution.

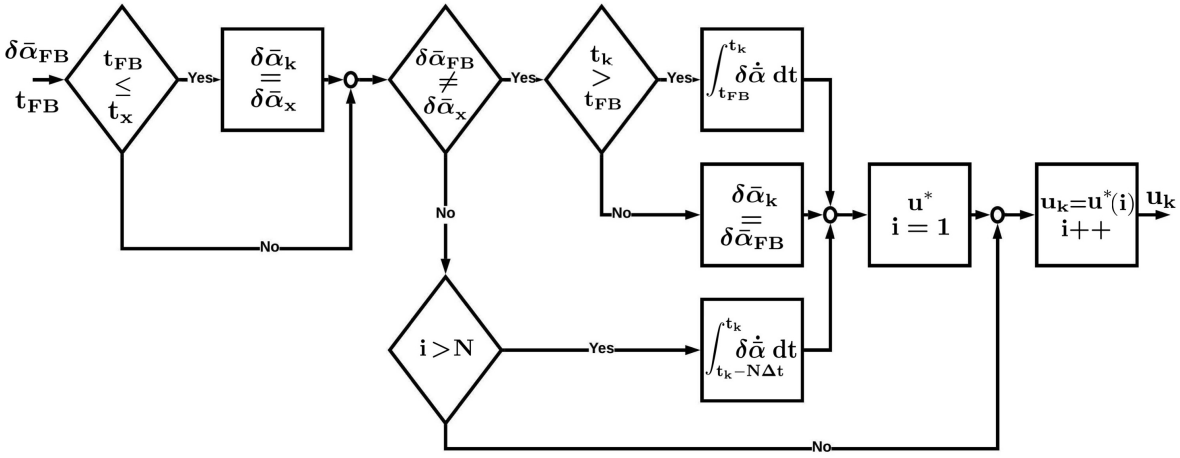

Figure 2. Block diagram representation of the delays/losses compensation structure.

CONTROLLER VALIDATION

Iterative algorithms for solution of nonconvex optimal control problems do not guarantee detection of the global optimum and may fall into local minima which are fairly distant from the optimum. To increase reliability of the solution in terms of optimality, a warm start strategy is adopted, which consists of using the global optimum of the convexified problem as first guess of the actual nonconvex OCP solution. $\boldsymbol{u}_0$* is the optimum of the convex OCP, obtained replacing the nonlinear dynamics with the linearized model, and running the algorithm with high number of iter-

ations. If the linearized model is accurate enough, the nonconvex OCP minimum, albeit local, will be close to the global optimum. Particularly suitable for nonconvex OCP, Lagrangian augmented gradient-based algorithms provide iterative solution to optimization problems characterized by nonlinear dynamics and nonlinear equality/inequality constraints. Among the open-source solutions implementing this approach, the GRAdient based MPC (GRAMPC) software, being designed for embedded applications, has been chosen as tool for solution of the OCP. GRAMPC, which is implemented in C language, allows the user to control the required computational power and execution time by fixing the maximum number of iterations for the gradient minimization and multipliers and penalties update loops. The networked controller validation relies on the SLAB Satellite Software (S3) toolkit for high-fidelity orbit propagation accounting for atmospheric drag, earth oblateness, solar radiation pressure, sun/moon attraction, relativity effects.[27]

Reliability of the control solution is verified through targeted analyses. Fuel efficiency is assessed performing a comparison between the MPC solution and the closed-form fuel-optimal solution developed in Reference 25. The efficacy of the d-term in allowing further ΔV reduction is evaluated analyzing the MPC solution for a given scenario when the d-term is active and inactive. The delays/losses compensation structure has been tested simulating faults of different lengths during the TOM triple pendulum acquisition maneuver.[3] Finally, a comparison of the solution obtained using the nonlinear and linear dynamics is presented.

Fuel Efficiency Analysis and d-term Validation

In Reference 25, Chernick et. al. develop a fuel-optimal impulsive closed-form solution which provides magnitude, sign and location of impulse(s) for in-plane and out-of-plane reconfigurations for unperturbed eccentric and perturbed near-circular reference orbits. Out-of-plane maneuvers can be achieved through a single impulse executed in proximity of an optimal location t_m, which is a parametric function of the integer variable k. The in-plane maneuver is accomplished using three impulses implemented at locations uniquely defined assigning three integer values to the variable k. Table 1 provides details of the two in-plane and out-of-plane maneuvers in near-circular reference

Table 1. In-plane and out-of-plane maneuvers characterization, simulation data and ΔV consumption.

Data	In-plane	Out-of-plane
Initial chief orbital elements	[6600km , 0.001, 0.140, 0, 0, 0]	[6828km, 0.00001, 1.361, 0, 0, 0]
Initial ROE state (m)	[30, 11000, 0, 50, 0, 0]	[0, 0, 273, 0, 10, 70]
Target ROE state (m)	[0, 10500, 45, 70, 0, 0]	[0, 0, 273, 0, 400, 120]
Closed-form k	(0, 1, 6)	0
Closed-form t_m $(orbits)$	[0.1840, 0.6856, 3.1929]	0.0107
MPC, $\lvert \boldsymbol{u}_{max} \rvert$ $(\frac{m}{s^2})$	32e-06	32e-06
Closed-form ΔV $(\frac{m}{s})$	[0.0094, -0.0460, 0.0192]	0.4373
MPC, d-term active $\lvert \Delta V \rvert$ $(\frac{m}{s})$	0.1476	0.5554
MPC, d-term inactive $\lvert \Delta V \rvert$ $(\frac{m}{s})$	0.1562	0.6439

orbit, chosen for the fuel-efficiency analysis and d-term validation.[25] For each maneuver the Table reports ΔV required for the closed-form and MPC solution with d-term active and inactive. Results of the two simulations in terms of control input trajectory (left) and ROE-space state evolution (right) are presented in Figure 3. The blue vertical lines represent location and sign of closed-form solution impulses. The green lines are multiples of the chosen optimal locations, obtained assigning increasing integers to the variable k. The two MPC solutions obtained activating and deactivating the d-term are indicated in black, respectively with a solid and dashed line. The in-plane MPC control trajectory is a sequence of impulses of finite width, having their peak in proximity of the

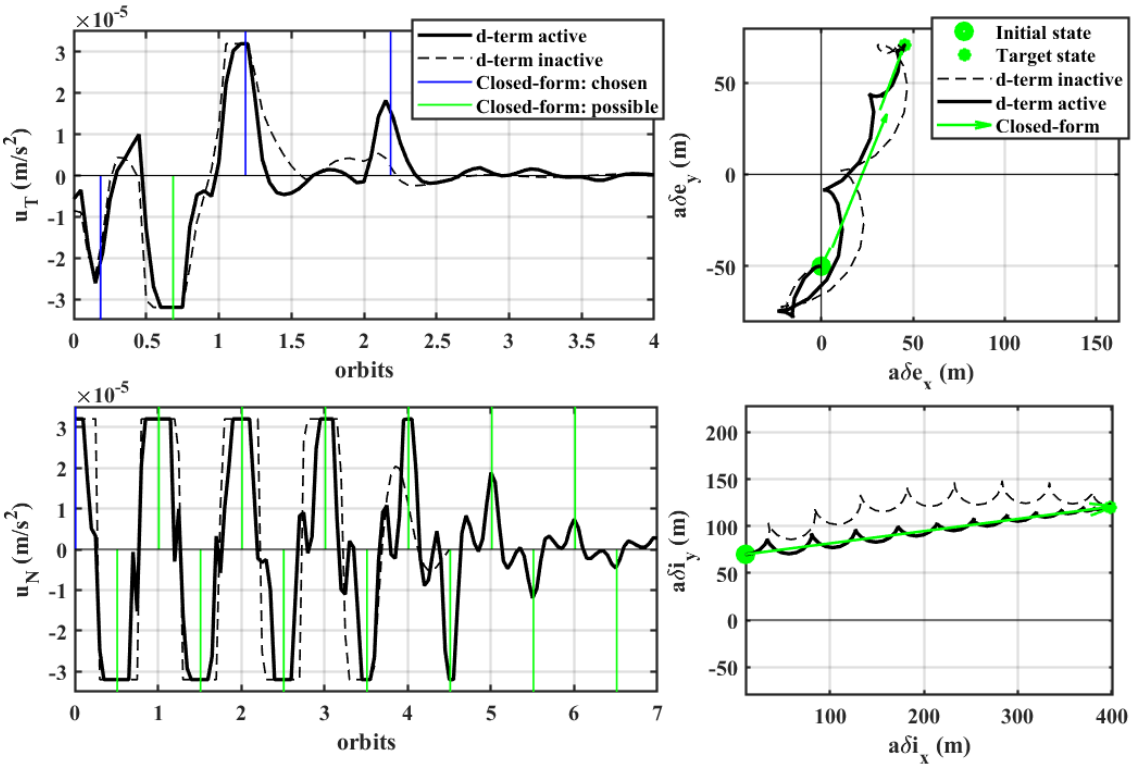

Figure 3. Comparison of control input profile and ROE-space trajectory for closed-form and MPC solutions with d-term active and inactive for in-plane and out-of-plane reconfigurations.

closed-form ideal impulses, which translates into a sequence of circle arcs in ROE-space. As visible in the plots, the size of the control acceleration impulse and the consequent arc in ROE-space are directly proportional. The closed-form ΔV's, given in Table 1, represent the maneuver ΔV lower bound. The analytical solution is not directly implementable in systems subject to continuous low-thrust requirements since the ideal impulses are required to be extremely narrow and high-thrust. The obtained continuous low-thrust solution distributes the ΔV along the orbit, widening impulses and reducing their magnitude to comply with the maximum thrust constraint, thus increasing the ΔV budget.

Benefits of including the d-term in the cost function are mostly evident in the cross-track maneuver (bottom plots). When the term is not active, the state trajectory in ROE-space is a sequence of equally-sized half circles, whose overall trend diverges from the straight line connecting initial and target state. The effect of forcing the trajectory to lie in the proximity of the straight line is evident when the term is active (solid line). In this case, the controller acts narrowing the impulses, reducing their size and increasing their number, as shown in the thrust profile. Table 1 shows that introduction of the d-term yields to a 14% ΔV reduction for the out-of-plane maneuver and 6% for the in-plane.

Delays/losses Compensation Structure Validation

This section aims at analyzing the behavior of a satellite subject to short and long faults during execution of a reconfiguration maneuver when the delays/losses compensation structure of Figure 2

is used.

Table 2. Triple pendulum acquisition scenario description, simulation data and faults definition.

Data	Value
Initial chief orbital elements	[7015km, 0.006766, 1.708, 5.569, 1.871, 1.85]
Initial ROE state (m)	[0, 88420, 0, 0, 0, 0]
Target ROE state (m)	[0, 85000, 0, 0, 0, 25000]
$\lvert \boldsymbol{u}_{max} \rvert$ ($\frac{m}{s^2}$)	120e-06
T ($orbits$)	5
Short fault start-end ($orbits$)	10-14
Long fault start-end ($orbits$)	10-49

The simulated scenario adopted in this analysis refers to the TOM mission triple-pendulum formation acquisition maneuver, starting from a string of pearls, whose data is reported in Table 2 together with the faults' characteristics. The prediction horizon T is 5 orbits, discretized in 150 steps. The faults are respectively 4 and 39 orbits long, chosen to be respectively shorter and longer than T. Figure 4 shows the cross-track acquisition in nominal operations (dashed black line) and

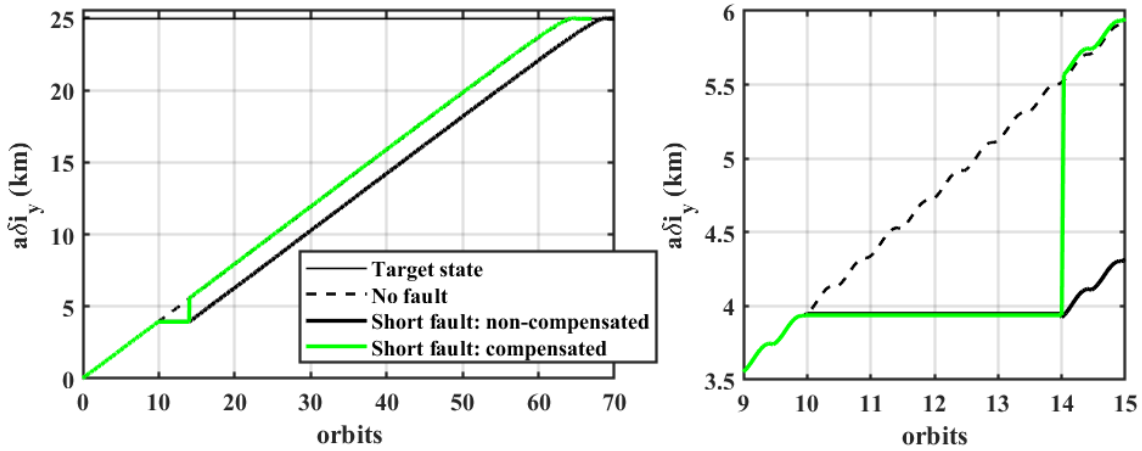

Figure 4. Comparison of δi_y acquisition in nominal operations (dashed black line) and in presence of a 4-orbit-long fault when the compensation structure is active (green line) and inactive (black solid line).

in presence of the short fault when the compensation structure is active (green line) and inactive (black solid line). The state behavior in the vicinity of the fault is highlighted in the right plot. From orbit 10 to 14 the controller operates in open-loop and implements, at each time-step, the last calculated optimal solution $\boldsymbol{u}^*$, as seen in the block diagram of Figure 2. This translates into the flat trend observable in Figure 4. The green line discontinuity indicates that, at the end of the fault, the measured state coincides with the value that it would have in nominal conditions (black dashed line). It follows that the $\boldsymbol{u}^*$ control solution implemented during the open-loop phase resembles the control trajectory calculated in nominal operations. To better visualize this result, Figure 5 provides a representation of the $\boldsymbol{u}_N$ control trajectory in two time domains. For a given simulation timestep, the plot provides the calculated optimal trajectory $\boldsymbol{u}_N{}^*$ for the length of the prediction horizon. An advancement towards positive values of simulation time translates into a shift towards the left in prediction horizon time. In nominal conditions only the simulation time trajectory is implemented. In case of a fault, when the latter is not available, the controller implements the trajectory in prediction horizon time. Since the differences between the two trajectories are hardly noticeable, the fault

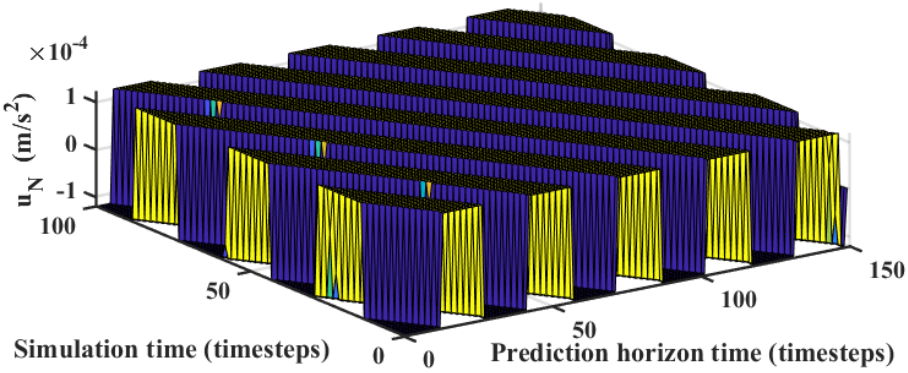

Figure 5. Simultaneous representation of the cross-track control input trajectory in prediction horizon time and simulation time.

is successfully compensated. If the fault is larger than the prediction horizon the same strategy is repeated multiple times. After implementing the last element of the optimal control solution $\boldsymbol{u}^*$, an estimate of the state is obtained integrating the model, and the new estimate used to provide a new optimal solution $\boldsymbol{u}^*$. Figure 6 shows the effect of a 39-orbit long fault, starting from orbit 10, on the δi_y trajectory in time (right) and in $\delta \boldsymbol{i}$-space (left). The blue circles highlight the state estimates, calculated at the end of each $\boldsymbol{u}^*$, whose values approximately match the measured state in absence of fault (black solid line). Table 3 provides an overall comparison between the previously discussed

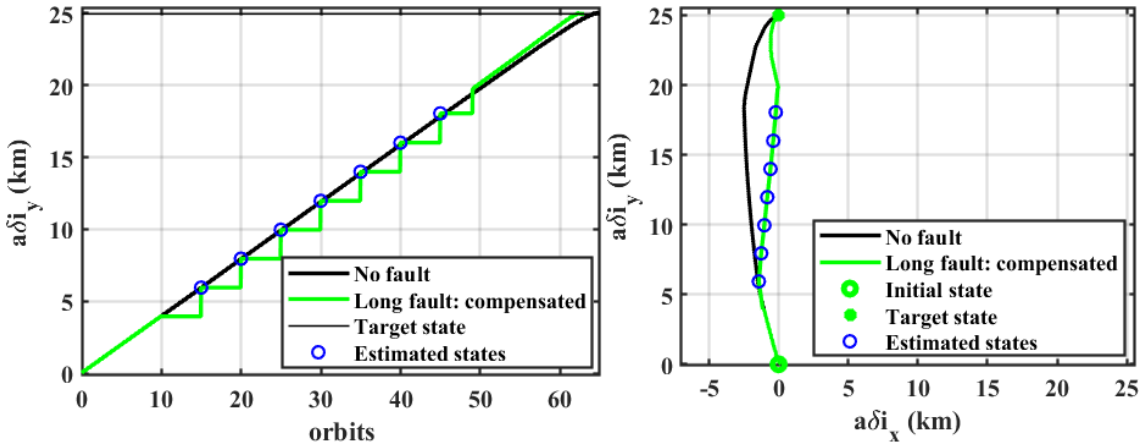

Figure 6. δi_y acquisition during nominal operations (thick black line) and in presence of a 39-orbit-long fault when the compensation structure is active (green line), in time domain (left) and $\delta \boldsymbol{i}$-space (right).

cases in terms of ΔV and maneuvering time. The total maneuvering time in absence of faults is 65 orbits. When the short and long faults are introduced and compensated, the maneuvering time remains within this range, dropping to 63 for the compensated long fault. If no compensation strategy is applied, the length of the maneuver increases respectively to 70 and 106 orbits. Referring to the 39-orbit-long fault, the satellite needs 43 more orbits, compared to the compensated case, to converge to the target, translating into 14 extra orbits needed to compensate for the accumulated drift. The use of the compensation structure yields to a ΔV reduction of 0.27 m/s, for the short fault, and 3.04 m/s, for the long fault.

Table 3. Comparison of ΔV consumption and maneuvering time for the triple pendulum acquisition maneuver, executed in nominal operations and in presence of a 4-orbit-long and a 39-orbit-long fault.

Case	ΔV (m/s)	Maneuvering time (orbits)
No Fault - Synchronous	45.55	65
Fault $<$ T - compensated	45.50	65
Fault $<$ T - non-compensated	45.77	70
Fault $>$ T - compensated	43.89	63
Fault $>$ T - non-compensated	46.93	106

Nonlinear and Linear Model Comparison

In this section, the quasi-nonsingular ROE-based linear model presented in Reference 21 and adopted in Reference 26 has been incorporated in the MPC, and its solution used as term of comparison for the nonlinear MPC solution. The reconfiguration scenario is a 505 km-diameter Projected Circular Orbit (PCO) acquisition starting from a 500 km-diameter PCO. Table 4 summarizes the reconfiguration data, simulation parameters and provides the total ΔV required by the linear and nonlinear MPC. The behavior of the two ROE components involved in the reconfiguration, δe_y and

Table 4. 505 km-diameter PCO formation acquisition data, simulation parameters and ΔV consumption.

Data	value
Initial ROE state (m)	[0, 0, 0, 129101,-258198, 0]
Target ROE state (m)	[0, 0, 0, 130225,-260446, 0]
Initial chief orbital elements	[7015km, 0.006766, 1.708, 5.569, 1.871, 1.85]
Maximum control acceleration ($\frac{m}{s^2}$)	120
Nonlinear $\Delta V(\frac{m}{s})$	4.7949
Linear $\Delta V(\frac{m}{s})$	4.7993

δi_x, is shown in Figure 7. The difference between the nonlinear solution (green solid line) and the linear (black dashed line) is barely noticeable. Table 4 confirms the similarities between the two

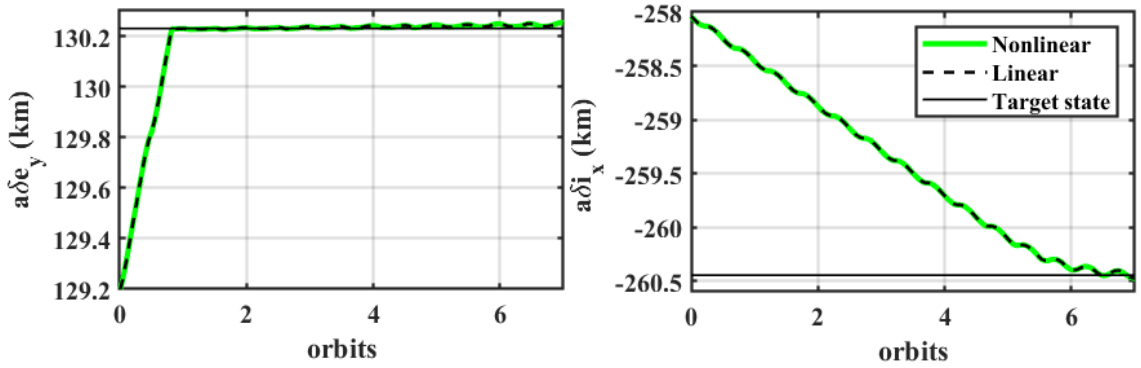

Figure 7. Linear and nonlinear MPC solutions comparison in terms of δe_y and δi_x trajectories for a 505 km-diameter PCO formation acquisition maneuver.

solutions, showing that the use of the nonlinear MPC leads to a saving of 0.0044 m/s.

Targeted analyses have been performed to validate the networked MPC thoroughly. The MPC solution has shown fuel-efficiency features as result of its comparison with a closed-form optimal solution and analysis of the benefits of introducing the novel d-term in terms of ΔV savings. The delays/losses compensation structure has been proven to efficiently guarantee convergence to the

target state, within the given ΔV and time budget, in case of unexpected faults. The comparison between linear and nonlinear MPC showed that the use of a nonlinear model does not lead to dramatic improvements in terms of ΔV consumption. Such similarities between the models reflect the inclusion of only secular perturbations effects in the GVEs, where the osculating component is neglected. Including perturbations as acceleration components during the model derivation would lead to a higher degree of accuracy, i. e. higher performance of the nonlinear MPC. Moreover, differences between the two solutions would result more prominent if a linear model based on relative position and velocity had been used.

CONCLUSION AND FUTURE WORK

A model predictive control (MPC) solution, based on relative orbital elements (ROE), for networked architectures of small satellites flying in low earth orbit (LEO) formations was presented. The work carries two main contributions to the state of the art: insertion of the perturbed nonlinear relative dynamic model, valid for reference orbits of arbitrary eccentricity, in the optimal control problem and inclusion of a novel term (d-term) in the cost function which allows exploitation of the latest theoretical results in terms of the properties of fuel-optimal trajectories in ROE-space. The model dynamics and the knowledge of the optimal control solution for the prediction horizon length allow robustness against delays, losses and long faults, through design of a specific compensation architecture. Given the difficulties in adopting conventional stability arguments for the time-variant uncertain nonconvex optimization problem, MPC stability and the optimal control problem (OCP) feasibility are obtained through imposition of a Lyapunov inequality constraint. A high-fidelity simulation environment has been set to closely resemble the true behavior of the satellite in space and the algorithm implementation on embedded hardware. Targeted analyses have been performed to validate the controller. The MPC solution has shown a fuel-optimal behavior, when compared to a closed-form solution, with further ΔV reduction when the d-term is active, whilst the compensation structure has demonstrated ability of open-loop operation for several orbits without exceeding the ΔV or time budget. In order to improve nonlinear model performances, future works may derive the model in a way to consider osculating effects of orbit perturbations, e. g. defining the acceleration vector appearing in the GVEs as the sum of J2, differential drag and control contributions. Validation of the improved MPC version should include comparison with a linear MPC based on relative position and velocity. Extension of this work to equatorial orbits could be achieved employing the modified equinoctial orbit elements as a replacement for the quasi-nonsingular ROE.[5,21] Further improvements may involve fuel-optimal locations reformulation in the Lyapunov constraint, which currently refer to unperturbed near-circular reference orbits, according to definitions more descriptive of eccentric reference orbits. In the guidance, navigation and control framework, the Networked MPC presented in this paper provides solution only to the control problem, since no collision avoidance has been included. The controller could benefit from extensions focused at developing and integrating a guidance layer which ensures a collision-free path among elements of a multi-satellite formation. The guidance strategy could be rather independent from the control layer, as in a path-planning approach, or alternatively, it could be incorporated in the objective function through collision terms whose weights increase with the inverse of satellites' distance. The networked nature of MPC makes it particularly suitable for swarms applications, if implemented in a centralized fashion, i. e. including concatenation of all the agents' states in the MPC state vector. A possible swarm scenario consists of a single mothership coordinating multiple agents, with limited computational resources, i. e. accommodating mainly sensors and actuators. Real-time agent-mothership communication is aimed to sensors/actuators data exchange for the sake of

control input calculation on the mothership side. Delays and losses of information affecting the communication would easily be compensated by the given structure and passive collision avoidance could be easily achieved by proper swarm design.[28]

ACKNOWLEDGEMENT

Ideas and motivation behind this work have been inspired by research developed under the German Aerospace Center (DLR) * grant number 50RA1733. The authors acknowledge the Space Rendezvous Lab (SLAB) for the precious support throughout the research activity.

REFERENCES

[1] S. D'Amico, M. Pavone, S. Saraf, A. Alhussien, T. Al-Saud, S. Buchman, R. Byer, and C. Farhat, "Miniaturized Autonomous Distributed Space System for Future Science and Exploration," *International Workshop on Satellite Constellations and Formation Flying*, International Astronautical Federations Astrodynamics Committee Delft, The , 2015, pp. 1–20.

[2] K. Schilling, P. Bangert, S. Busch, S. Dombrovski, A. Freimann, A. Kramer, T. Nogueira, D. Ris, J. Scharnagl, and T. Tzschichholz, "Netsat: a four pico/nano-satellite mission for demonstration of autonomous formation flying," *66th International Astronautical Congress*, 2015.

[3] K. Schilling, T. Tzschichholz, M. Motroniuk, A. Aumann, I. Mammadov, O. Ruf, C. Schmidt, N. Appel, A. Kleinschrodt, S. Montenegro, *et al.*, "TOM: A Formation for Photogrammetric Earth Observation by Three Cubesats," *4th IAA Conference on University Satellite Missions and CubeSat Workshop, Rome, Italy*, 2017.

[4] A. W. Koenig, B. Macintosh, and S. D'Amico, "Formation Design of Distributed Telescopes in Earth Orbit for Astrophysics Applications," *Journal of Spacecraft and Rockets*, 2019, pp. 1–16.

[5] N. Stacey and S. D'Amico, "Autonomous Swarming for Simultaneous Navigation and Asteroid Characterization," *AAS/AIAA Astrodynamics Specialist Conference*, 2018.

[6] D. Q. Mayne, "Model predictive control: Recent developments and future promise," *Automatica*, Vol. 50, No. 12, 2014, pp. 2967–2986.

[7] J. B. Rawlings and D. Q. Mayne, *Model predictive control: Theory and design*. Nob Hill Pub. Madison, Wisconsin, 2009.

[8] D. Q. Mayne, J. B. Rawlings, C. V. Rao, and P. O. Scokaert, "Constrained model predictive control: Stability and optimality," *Automatica*, Vol. 36, No. 6, 2000, pp. 789–814.

[9] A. Weiss, M. Baldwin, R. S. Erwin, and I. Kolmanovsky, "Model predictive control for spacecraft rendezvous and docking: Strategies for handling constraints and case studies," *IEEE Transactions on Control Systems Technology*, Vol. 23, No. 4, 2015, pp. 1638–1647.

[10] S. Di Cairano, H. Park, and I. Kolmanovsky, "Model predictive control approach for guidance of spacecraft rendezvous and proximity maneuvering," *International Journal of Robust and Nonlinear Control*, Vol. 22, No. 12, 2012, pp. 1398–1427.

[11] J. Scharnagl, P. Kremmydas, and K. Schilling, "Model Predictive Control for Continuous Low Thrust Satellite Formation Flying," *IFAC-PapersOnLine*, Vol. 51, No. 12, 2018, pp. 12–17.

[12] L. Sauter and P. Palmer, "Analytic model predictive controller for collision-free relative motion reconfiguration," *Journal of Guidance, Control, and Dynamics*, Vol. 35, No. 4, 2012, pp. 1069–1079.

[13] M. Leomanni, E. Rogers, and S. B. Gabriel, "Explicit model predictive control approach for low-thrust spacecraft proximity operations," *Journal of Guidance, Control, and Dynamics*, Vol. 37, No. 6, 2014, pp. 1780–1790.

[14] R. Larsson, S. Berge, P. Bodin, and U. T. Jönsson, "Fuel efficient relative orbit control strategies for formation flying and rendezvous within PRISMA," *Guidance and Control 2006, 4-8 February 2006, Breckenridge, CO, USA*, Univelt Inc., USA, 2006, pp. 25–40.

[15] E. N. Hartley, P. A. Trodden, A. G. Richards, and J. M. Maciejowski, "Model predictive control system design and implementation for spacecraft rendezvous," *Control Engineering Practice*, Vol. 20, No. 7, 2012, pp. 695–713.

[16] T. Englert, A. Völz, F. Mesmer, S. Rhein, and K. Graichen, "A software framework for embedded nonlinear model predictive control using a gradient-based augmented Lagrangian approach (GRAMPC)," *arXiv preprint arXiv:1805.01633*, 2018.

*Deutsche Zentrum für Luft und Raumfahrt (DLR)

[17] D. C. Panagiotis, J. Liu, and D. M. d. l. Pena, *Networked and Distributed Model Predictive Control. Methods and Nonlinear Process Network Applications*. Springer, 2011.

[18] S. D'Amico and O. Montenbruck, "Proximity operations of formation-flying spacecraft using an eccentricity/inclination vector separation," *Journal of Guidance, Control, and Dynamics*, Vol. 29, No. 3, 2006, pp. 554–563.

[19] S. D'Amico, *Autonomous formation flying in low earth orbit*. PhD thesis, TU Delft, Delft University of Technology, 2010.

[20] S. D'Amico, "Relative orbital elements as integration constants of Hills equations," *DLR, TN*, 2005, pp. 05–08.

[21] A. W. Koenig, T. Guffanti, and S. D'Amico, "New State Transition Matrices for Relative Motion of Spacecraft Formations in Perturbed Orbits," *AIAA/AAS Astrodynamics Specialist Conference*, 2016, p. 5635.

[22] J. L. Junkins and H. Schaub, *Analytical mechanics of space systems*. American Institute of Aeronautics and Astronautics, 2009.

[23] F. Borrelli, A. Bemporad, and M. Morari, *Predictive control for linear and hybrid systems*. Cambridge University Press, 2017.

[24] S. Boyd and L. Vandenberghe, *Convex optimization*. Cambridge university press, 2004.

[25] M. Chernick and S. D'Amico, "New closed-form solutions for optimal impulsive control of spacecraft relative motion," *AIAA/AAS Astrodynamics Specialist Conference*, 2016, p. 5659.

[26] L. M. Steindorf, S. D'Amico, J. Scharnagl, F. Kempf, and K. Schilling, "Constrained Low-Thrust Satellite Formation-Flying using Relative Orbit Elements," *27th AAS/AIAA Space Flight Mechanics Meeting*, 2017.

[27] V. Giralo and S. D'Amico, "Development of the Stanford GNSS Navigation Testbed for Distributed Space Systems," *Institute of Navigation, International Technical Meeting*, Inst. of Navigation Reston, VA, 2018, pp. 837–856.

[28] A. W. Koenig and S. D'Amico, "Robust and Safe N-Spacecraft Swarming in Perturbed Near-Circular Orbits," *Journal of Guidance, Control, and Dynamics*, Vol. 41, No. 8, 2018, pp. 1643–1662.